Bioactive Materials 5 (2020) 624–635

Contents lists available at ScienceDirect

Bioactive Materials

journal homepage: http://www.keaipublishing.com/biomat

High-affinity mutant Interleukin-13 targeted CAR T cells enhance delivery of clickable biodegradable fluorescent nanoparticles to glioblastoma

Gloria B. Kim[a], Virginia Aragon-Sanabria[a], Lauren Randolph[a], Hali Jiang[a], Joshua A. Reynolds[a], Becky S. Webb[b], Achuthamangalam Madhankumar[b], Xiaojun Lian[a], James R. Connor[b,**], Jian Yang[a,*], Cheng Dong[a,***]

[a] Department of Biomedical Engineering, The Pennsylvania State University, University Park, PA, 16802, United States
[b] Department of Neurosurgery, M. S. Hershey Medical Center, The Pennsylvania State University, Hershey, PA, 17033, United States

ARTICLE INFO

Keywords:
Glioblastoma
T cells
Nanoparticles
Targeted drug delivery
Citrate polymers
Fluorescence

ABSTRACT

Glioblastoma (GBM), the deadliest form of brain cancer, presents long-standing problems due to its localization. Chimeric antigen receptor (CAR) T cell immunotherapy has emerged as a powerful strategy to treat cancer. IL-13-receptor-α2 (IL13Rα2), present in over 75% of GBMs, has been recognized as an attractive candidate for anti-glioblastoma therapy. Here, we propose a novel multidisciplinary approach to target brain tumors using a combination of fluorescent, therapeutic nanoparticles and CAR T cells modified with a targeted-quadruple-mutant of IL13 (TQM-13) shown to have high binding affinity to IL13Rα2-expressing glioblastoma cells with low off-target toxicity. Azide-alkyne cycloaddition conjugation of nanoparticles to the surface of T cells allowed a facile, selective, and high-yielding clicking of the nanoparticles. Nanoparticles clicked onto T cells were retained for at least 8 days showing that the linkage is stable and promising a suitable time window for *in vivo* delivery. T cells clicked with doxorubicin-loaded nanoparticles showed a higher cytotoxic effect *in vitro* compared to bare T cells. *In vitro* and *in vivo* T cells expressing TQM-13 served as delivery shuttles for nanoparticles and significantly increased the number of nanoparticles reaching brain tumors compared to nanoparticles alone. This work represents a new platform to allow the delivery of therapeutic nanoparticles and T cells to solid tumors.

1. Introduction

It is well recognized that very few existing polymeric nanoparticles (NPs) are truly specific for tumor targeting after intravenous injection and the targeting still relies on passive mechanisms like the enhance permeability and retention effect (EPR). In contrast to cells, NPs lack an active mechanism to migrate across biological barriers. Particularly, the blood-brain barrier (BBB) poses a tremendous challenge for targeted delivery of therapeutics to the central nervous system (CNS). Glioblastoma multiforme (GBM) is one of the most aggressive types of tumors in the CNS. Despite major research efforts, the survival rate after 5-years is still less than 5% [1,2]. Current standard of care for newly diagnosed patients includes maximal surgical resection followed by a 6-week course of radiotherapy and systemic administration of temozolomide [3]. GBM is extremely challenging to treat because many drugs fail to efficiently cross the BBB and often times the tumor infiltrates areas of the brain that are hard to operate and tumor margin delimitation during surgery is commonly inaccurate [4].

T cells were shown to infiltrate solid tumors more than three decades ago [5], and their therapeutic potential was recognized as early as 1988, when significant tumor regression was reported in patients with metastatic melanoma that were treated with a combination therapy of autologous tumor infiltrating lymphocytes (TILs) and interleukin (IL)-2 [6]. However, it is now known that the immunosuppressive tumor microenvironment prevents complete tumor clearance by TILs [7]. Modern versions of the adoptive cell therapy (ACT) approach use genetically engineered autologous T cells that express chimeric antigen receptors (CARs) to increase tumor specificity and cytotoxicity. CAR molecules are single chain antibodies that confer specificity on the extracellular side of T cells and are fused to intracellular signaling domains of T cell receptors (TCR) like CD3-ζ or FcR-γ for cell activation, as well as co-stimulatory domains like CD28, 4-1 B B or 0X-40 to

Peer review under responsibility of KeAi Communications Co., Ltd.
* Corresponding author.
** Corresponding author.
*** Corresponding author.
E-mail addresses: jconnor@pennstatehealth.psu.edu (J.R. Connor), jxy30@psu.edu (J. Yang), cxd23@psu.edu (C. Dong).

https://doi.org/10.1016/j.bioactmat.2020.04.011
Received 15 April 2020; Accepted 16 April 2020

support cell expansion [8]. Unprecedented clinical success has been seen in adoptive transfer of T cells expressing CARs targeting CD19 for treating patients with B-cell malignancies [9] and has raised optimism for the potential of ACT for the treatment of non-hematological cancers [10].

However, solid tumors present additional challenges. One of the biggest challenges to overcome is the effect of the extracellular proteins of the solid tumors which downgrade cytotoxic T cell activity [11]. To circumvent this potential problem, we developed NPs, which use T cell as delivery vehicles to reach the solid tumor environment and release the antineoplastic drug. In our model, we decided to use GBM as the cancer model. In the case of GBM, it is estimated that approximately 75% of tumors selectively overexpress the α2 subtype of the interleukin-13 receptor (IL-13Rα2) [18,19]. Efforts are underway to target the IL-13Rα2 with NPs [20,21] and CAR T cells [22–26] using the IL-13 peptide to guide targeting. However, IL-13 also binds to the interleukin-4 receptor α chain (IL-4R), the shared IL-13/IL-4 receptor, which has a much broader distribution in the body than IL-13Rα2. To minimize the potential off-target effects, we used a mutant version of IL-13 known as the targeted quadruple mutant-13 (TQM-13). TQM-13 contains four point mutations that improve its binding affinity to the IL-13Rα2 receptor ($K_d \sim 5$ nM), while decreasing affinity to the IL-13 receptor α1 subunit [27,28]. IL-13Rα2 expression is not exclusive of solid tumors, as the mRNA for this receptor has been detected in the testis [23], but experiments *in vivo* showed specific tumor targeting of TQM-13 in an orthotopic glioblastoma tumor model in mice producing little to no accumulation in the testis [21]. Therefore, using CAR T cells that express TQM-13 may represent a high affinity and low off-target toxicity specific drug delivery carrier for brain tumors and an important improvement over the current clinical strategies.

The purpose of this work is to develop a combined selective targeting system (TQM-13) with a unique clickable T cell-mediated NP drug delivery system CTNDDS that can overcome the immunosuppressive tumor microenvironment and address unmet challenges in cancer targeting and drug delivery, especially in the CNS. It is critical to have a mechanism that can kill cancer cells even in the context of an immunosuppressive microenvironment [24]. We hypothesize that by taking advantage of the targeting, penetrating, and therapeutic/biological functions of the TQM-13 CAR T cells combined with pH-sensitive, controlled release mechanism of drug-encapsulating NPs, our proof-of-concept CTNDDS has the potential to overcome significant challenges in the treatment of brain cancer. We demonstrate the feasibility of our approach by clicking nanoparticles onto primary human T cells, either untransduced or transduced with the TQM-13 CAR molecules. This is accomplished through a unique click chemistry method and pH-sensitive linkers that allow us to achieve controlled, targeted and stimuli-responsive delivery of an antitumor drug (doxorubicin)-loaded NPs from TQM-13 CAR T cells to brain tumor cells. Click chemistry enables immobilizing materials on cell surfaces through bioorthogonal reaction. N-azidoacetylmannosamine-tetraacylated (Ac4ManNAz) is an azide-containing sugar that can be metabolized by cells and incorporated into proteoglycans located on cell membranes. As this azide group is not naturally present on the extracellular side of the plasma membrane, the Ac4ManNAz sugar enables specific click labeling of viable cells once introduced in the media.

The clickable NPs were built upon biodegradable photobleaching-resistant fluorescent polymer (BPLP)-polylactide copolymers (BPLP-PLAs) [25–29]. Inherent photoluminescence of the BPLP-PLA polymer without conjugating photobleaching organic dyes or cytotoxic quantum dots enables the tracking of BPLP-PLA-NPs or cells carrying the NPs. This imaging property imparts an additional diagnostic modality to our therapeutic CTNDDS, which is often desired in the field of cancer therapy. The surface conjugation of NPs onto T cells can minimize the side effects to immune cells in contrast to loading particles into the cells. In addition, clicking modality with pH-sensitive linkers enables the controlled release of the NPs more effectively in the acidic tumor microenvironment. Taken together, the abovementioned attributes of this new, smart CTNDDS system raise hope for the treatment of brain tumor and other solid tumors with redirected T cells.

2. Materials and methods

2.1. Reagents

Chemicals for clickable BPLP-PLA synthesis were purchased from Sigma-Aldrich. Recombinant Human/Rhesus Macaque/Feline CXCL12/DSF-a alpha was purchased from R&D systems (R&D Systems, Minneapolis, MN, USA; catalog #: 350-NS). Hydrocortisone solution was purchased from Sigma Aldrich (Sigma-Aldrich, St. Louis, MO, USA; catalog #: H6909-10 mL). Attachment factor solution was purchased from Cell Applications (Cell Applications, San Diego, CA, USA; catalog #: 123-100). Histopaque was purchased from Sigma-Aldrich (Sigma-Aldrich St. Louis, MO, USA; catalog #: 10771). Red cell lysis buffer was purchased from Invitrogen (Invitrogen, Carlsbad, CA, USA; catalog #: A10492-01). TNF-α was obtained from Invitrogen (Invitrogen, Carlsbad, CA, USA; catalog #: PHC3015). Doxorubicin HCl was purchased from Enzo Life Sciences (Enzo Life Sciences, Farmingdale, NY, USA; catalog #: BML-GR319-0005). CCK-8 assay kit was purchased from Dojindo (Dojindo Molecular Technologies, Inc., Kumamoto, Japan). Firefly Luciferase Glow Assay Kit was purchased from Thermo Fisher Scientific (Thermo Fisher Scientific, Waltham, MA, USA; catalog #: 16176). Corning® Transwell® polycarbonate membrane cell culture inserts (6.5 mm Transwell with 5.0 μm pore polycarbonate membrane insert, TC-treated, w/lid, sterile, 48/cs) were purchased from Sigma-Aldrich (Sigma-Aldrich, St. Louis, MO, USA; catalog #: CLS3421). Human fibronectin was purchased from Corning (Corning, Corning, NY, USA; catalog #: 356008). ManNAz (molecular weight: 430.37) was purchased from Thermo Fisher Scientific (Thermo Fisher Scientific, Waltham, MA, USA; catalog #: P188904). Primary antibody (Hamster monoclonal anti -CD3 (1:200, Abcam catalog #: ab91497), rabbit polyclonal anti-Ki67 (1:200, Abcam catalog #: ab15580). Secondary antibody (goat anti-hamster 405 (1:200, Abcam catalog #: ab175680), and goat anti-rabbit 555 (1:200, Santa Cruz cat#A21430). Neutral red based *in vitro* toxicology assay was purchased from Sigma-Aldrich (Sigma-Aldrich, St. Louis, MO, USA; catalog #: TOX4-1 KT).

2.2. Cell culture

Bovine brain microvascular endothelial cells (BBMVEC; Cell Applications, San Diego, CA, USA; catalog #: B840-05) were cultured in plates pre-treated with attachment factor solution using bovine brain endothelial cell growth medium (Cell applications, San Diego, CA, USA; catalog #: B819-500). The cells were maintained in a 37 °C incubator with 5% CO2 and a relative humidity of 95%. The medium was changed every two or three days. For migration studies, the basal medium that contains no growth supplement (Cell applications, San Diego, CA, USA; catalog #: B818-500) was used. Human Jurkat cells, clone E6-1 (ATCC, catalog #: TIB-152) were cultured in complete RPMI-1640 medium (Invitrogen, Carlsbad, CA, USA; catalog #: 11875-135) supplemented with 10% fetal bovine serum (ATLANTA biologics, Flowery Branch, GA, USA; catalog #: S11150), and 1% antibiotic antimycotic 100X solution (Invitrogen, Carlsbad, CA, USA; catalog #: 15070-063) at 37 °C in a humidified incubator with 5% CO2. The medium was changed every three days. Human astrocytes or HAs (HA; ScienCell Research Laboratories, Corte Del Cedro, Carlsbad, CA, USA; catalog #: 1800) were received as a gift from Dr. Gong Chen (Pennsylvania State University, University Park, PA, USA) and maintained in astrocyte medium (ScienCell Research Laboratories, Carlsbad, CA, USA: catalog #: 1801) at 37 °C in a humidified atmosphere containing 5% CO2. These HAs were isolated from human cerebral cortex. Primary human T cells were routinely isolated from whole blood samples from healthy donors following the established IRB protocol # 31120 approved by the

Pennsylvania State University. Human T cells were cultured in ImmunoCult-XF T cell expansion media from StemCell Technologies (StemCell Technologies, Vancouver, Canada; catalog #: 10981) supplemented with 30 U/ml interleukin-2 (IL-2) from PeproTech (PeproTech, Rocky Hill, NJ, USA; Cat. No.: 200-02-10UG), 100 U/ml Penicillin and 100 μg/ml Streptomycin from Invitrogen (Invitrogen, Carlsbad, CA, USA; catalog #: 15070-063) and stimulated with anti-CD3/CD28 magnetic beads from Invitrogen (Invitrogen, Carlsbad, CA, USA; catalog #: 11161D), cells were maintained at 37 °C and 5% CO2 in a humidified incubator. Human U87Luc glioblastoma cell line was purchased from PerkinElmer (PerkinElmer, Waltham, MA USA: catalog #:124577) and transduced with luciferase (U87Luc) for viability quantification and IVIS imaging. The cell line was cultured in DMEM (Thermo Fisher Scientific, Waltham, MA, USA; catalog #: 11885-076) and supplemented with 10% fetal bovine serum (ATLANTA biologics, Flowery Branch, GA, USA: catalog #: S11150), and 1% antibiotic antimycotic 100X solution (Invitrogen, Carlsbad, CA, USA; catalog #: 15070-063) at 37 °C in a humidified incubator with 5% CO2. The medium was changed every three days. Human embryonic kidney 293 (HEK293) cells were maintained in DMEM from Thermo Fisher Scientific (Thermo Fisher Scientific, Waltham, MA, USA; catalog #: 10569010) supplemented with 10% FBS (VWR) and passaged every three to four days via Trypsin 0.25% EDTA from Invitrogen (Invitrogen, Carlsbad, CA, USA; catalog #: 25200-056) mediated dissociation. Cells were routinely tested to ensure mycoplasma free culture conditions using an established PCR based detection method [30].

2.3. Primary human T cell isolation, characterization and expansion

Healthy volunteers were directed to the Clinical Research Center (CRC) in University Park where fresh blood samples were taken through venipuncture and collected in tubes spray-dried with EDTA from BD (Cat. No.: 366643). Blood samples were transferred to the lab and immediately processed. Primary T cells were isolated from the fresh blood samples using histopaque-1077 according to manufacturer's instructions. Briefly, 3 ml of histopaque-1077 were transferred into a 15 ml, then 3 ml of blood were layered on top of the histopaque. Tubes were centrifuged at 400 g for 30 min at room temperature to create a buffy coat containing a cell layer enriched with T cells. After centrifugation, cells from the buffy coat where transferred to a new tube and washed with 10 ml of DPBS. Cells were centrifuged again at 250 g for 10 min at room temperature. Supernatant was aspirated out, cells were washed with 5 ml of DPBS and centrifuged at 250 g for 10 min at room temperature. The last step was repeated one last time. In the end, cells were resuspended in 1 ml of media and transferred on top of 10 ml of red cell lysis buffer to eliminate any red blood cells remaining in the sample. Cells were incubated with the lysis buffer for 4 min at room temperature and then centrifuged at 300 g for 5 min. Supernatant was aspirated out and cells were resuspended in 10 ml of media.

To characterize T cells after isolation we used flow cytometry to measure the subpopulation of cells expressing CD3. For this purpose, cells were stained with anti-CD3 antibody from Invitrogen (Invitrogen, Carlsbad, CA, USA; catalog #: 14-0038-80) followed by an Alexa-Fluor 488 tagged goat anti-mouse secondary antibody from Invitrogen at a 1:1000 dilution (Invitrogen, Carlsbad, CA, USA; catalog #: A-11017). $CD3^+$ expression was measured right after cell isolation and after one-week cell culture. Results were analyzed with Flow Jo.

To stimulate the proliferation of T cells *in vitro*, we used anti-CD3/CD28 Dynabeads for T cell expansion (Invitrogen, Carlsbad, CA, USA; catalog #: 11161D). Cells were counted and seeded in 6-well plates at a density of 5×10^5 cells/well and incubated with beads at a 1:2 bead to cell ratio. Cells were incubated for 5 days, counted again and passaged to maintain a constant bead to cell ratio. Primary cells were routinely maintained for 3 weeks and then a new batch of fresh cells was isolated.

2.4. Synthesis of clickable BPLP-PLA polymer and pH-sensitive linkers

BPLP was synthesized by using citric acid, 1,8-octanediol, and L-serine, as previously reported [31]. BPLP-PLA copolymer with intrinsic fluorescence was synthesized and fabricated as previously reported [32]. Varying the BPLP to L-lactide molar ratio allows control over the degradation rate. A BPLP to L-lactide ratio of 1:50 was used in this study to ensure minimal degradation within the time range of our study. In order to fabricate clickable nanoparticles with pH-sensitive linkers, 10 g of BPLP-PLA polymer was dissolved in 50 mL of chloroform. 10 mL of hydrazine hydrate was added and the mixture was stirred for 3 h 200 mL of 1:1 mixture of ethanol:water was added. Rotary evaporator was used to completely dry and remove unreacted hydrazine hydrate. The dried powder was dissolved in 20 mL of ethanol. 3 mL triethylamine (or TEA) and 20 mL 50% glutaraldehyde were added to the mixture and the mixture was stirred overnight. The mixture was then concentrated using a rotary evaporator and precipitated in DI water, followed by freeze-drying. To synthesize clickable succinic dihydrazide or pH-sensitive linkers, 0.5 g propiolic acid and 0.77 g EDC (or 0.95 g of EDC.HCl) were dissolved in 20 mL MES and the mixture was stirred for 1 h before 0.57 g of NHS was added to the mixture. After the mixture was stirred for 1 h, 0.8 g succinic dihydrazide was added and the mixture was stirred again for 48 h. The linkers were obtained after freeze-drying.

2.5. BPLP-PLA nanoparticle fabrication and characterization

Clickable BPLP-PLA nanoparticles were prepared by the single emulsion method. Briefly, 50 mg BPLP-PLA polymer was dissolved in 2 mL chloroform solution, which was added drop-wise into the mixture containing 20 mL 5 wt% poly (vinyl alcohol) (87% hydrolyzed, MW 87 kDa) and 50 mg pH-sensitive linkers during sonication. The solution was stirred vigorously for 4 h for solvent evaporation. Resulting BPLP-PLA nanoparticles were centrifuged at 12,000 rpm and washed with deionized (DI) water for three times before lyophilized. Clickable doxorubicin drug loaded nanoparticles (Dox-BPLP-PLA-NP) were prepared by dissolving 10 wt% (with respect to the weight of BPLP-PLA polymer) of DOX in 1 mL DMSO and mixing with the polymer solution, followed by the same single emulsion and washing procedure to obtain drug loaded nanoparticles. Dox-BPLP-PLA-NP were washed using DI water for three times before lyophilized as well. The particle size, size distribution, and zeta potential were measured by DLS (Malvern Zetasizer ZS).

2.6. Clicking cells with nanoparticles

50 μM of Ac4ManNAz (reconstituted in DMSO) was used to treat primary human T cells for 3 days. After the treatment, the cells were washed with DPBS three times to remove free Ac4ManNAz. 2×10^6 cells were treated with 1 mg of clickable BPLP-PLA-NP or clickable Dox-BPLP-PLA-NP, 15 μg of sodium ascorbate, and 5 μg of CuCl in 2 mL of DPBS at 37 °C for 30 min on a rocker. Afterwards, the cells were washed gently with DPBS three times and then subjected to further characterization and studies.

2.7. Nanoparticle clicking efficiency on primary human T cells using flow cytometry

Following nanoparticle clicking onto T cells, samples were washed gently with DPBS for three times, and then subjected to flow cytometry analysis using a Guava® easyCyte Flow Cytometer (EMD Millipore); data analysis was performed with FlowJo v.10. T cells alone were used as control samples to establish fluorescence background.

2.8. Cytotoxicity assays

Cytotoxicity of BPLP-PLA-NPs, Dox-BPLP-PLA-NPs, T cells and T cells clicked with Dox-BPLP-PLA-NPs were evaluated by adding cells alone or cells clicked with Dox-BPLP-PLA-NPs at different numbers into 48 well plates with U87Luc cells (cell seeding density = 25000 cells per well). After 48 h of incubation, the cells were washed with DPBS twice and treated with 100 μL of 1X cell lysis buffer. After the cells were lysed, 20 μL of the cell lysate from each well were added to a white 96-well plate. To each well, 50 μL of Luciferase working solution was added. After 10 min of incubating the plate in the dark, the light output from each well was measured using a microplate reader (TECAN, infinite M200 PRO).

2.9. Brain endothelial barrier disruption assay

BBMVECs were grown until confluency on 25 mm round No. 1 glass coverslips coated with 1 mg/ml fibronectin and activated with TNF-α (25 ng/ml) for 6 h in order to mimic the inflammatory condition in the brain prior to the experiment. T cells were added on top of BBMVECs and incubated for 90 min. After the incubation, unbound T cells were washed away, and the coverslips were fixed in 4% formaldehyde for 15 min. Cells were then treated with a permeabilization/blocking buffer containing 5% Goat Serum from Sigma-Aldrich (Sigma-Aldrich, St. Louis, MO, USA; catalog #: G6767) and 0.3% Triton X-100 from Sigma-Aldrich (Sigma-Aldrich, St. Louis, MO, USA; catalog #: X100) in 1 × DPBS for 1 h at room temperature. Cells were then incubated with a primary antibody for VE-cadherin from Cell Signaling at a 1:300 dilution (Cell Signaling, Danvers, MA, USA; catalog #: 2500), in an antibody dilution buffer containing 1% bovine serum albumin (BSA) from VWR (VWR, Radnor, PA, USA; catalog #: 97061-144) and 0.3% Triton X-100 in DPBS over night at 4 °C. Cells were then washed three times in DPBS and incubated with an Alexa-Fluor 488 tagged goat anti-mouse secondary antibody from Invitrogen at a 1:1000 dilution (Invitrogen, Carlsbad, CA, USA; catalog #: A-11017), in antibody dilution buffer for 1 h at room temperature protected from light. Cells were then washed three times in DPBS and counterstained with Hoechst from Invitrogen (Invitrogen, Carlsbad, CA, USA; catalog #: H3570) as per manufacturer's instructions. Finally, glass coverslips were mounted on microscope slides using Fluoromount-G from Southern Biotech (Southern Biotech, Birmingham, AL, USA; catalog #: 0100-01) before imaging. Images were acquired using a Nikon Eclipse Ti-E inverted microscope equipped with a Photometrics CoolSNAP HQ2 CCD camera and a 100 × oil objective. Using a grid of 6 by 4, a total of 24 images were captured per cover glass. Gap percentage measurements were determined as the area not covered by BBMVECs (gaps) divided by the total area of each image and multiplied by 100. Analysis was performed using Image J software.

2.10. In vitro BBB model, characterization and cell migration

First, astrocytes were seeded onto the abluminal side of the Transwell membranes (5 μm pore size) pre-coated with 1 mg/ml of fibronectin and allowed to adhere for 2 h and grow for 2–3 days. When 80% confluence was reached, the inserts were turned over and placed inside the plates. With the astrocytes under the membrane, 1×10^4 BBMVECs were seeded on the upper chamber. Both cell lines were cultured until they reached full confluence. In the last 2 days of the culture, 100 nM of hydrocortisone was added to the medium to increase the expression of tight junctions in the brain endothelial cells and seal the barrier. To confirm the integrity of the BBB, FITC-dextran MW 40 kDa was added to the top chamber and allowed to diffuse across the BBB. After 4 h, samples from the bottom chambers were collected and analyzed using a microplate reader (TECAN, infinite M200 PRO). Fluorescence was compared between naked inserts and inserts containing BBMVECs and astrocytes incubated for the same period of time.

For migration experiments, BBB monolayers were activated with TNF-α (25 ng/ml) for 6 h. After the BBB activation with a pro-inflammatory TNF-α. To evaluate the migration, 2.5×10^4 cells in 100 μl of RPMI medium with low serum were placed in the upper chambers, and the lower chambers were filled with 600 μl of the mixture of low-serum medium and chemoattractant (500 ng/mL of C-X-C motif chemokine ligand (CXCL)-12 CXCL-12). After 4 h at 37 °C, the media in the upper chambers was aspirated and the top of the membrane was scraped gently with cotton tips. Migrated cells on the abluminal side of the Transwell were collected and counted using a hemocytometer. Percentage of migration was determined based on the number of immune cells recovered from the lower compartment and the total number of immune cells initially added to the system. The membranes were retrieved and fixed for confocal imaging to image the immune cells in the process of transmigration.

2.11. Intracranial xenograft model

All murine protocols were reviewed and approved by the Institutional Animal Care and Use Committee (IACUC) at Penn State University under the protocol number PRAMS201546647. All experiments were performed in accordance with relevant guidelines and regulations in the state of Pennsylvania. Female immunodeficient nude mice (strain 088, Charles River Laboratories, Wilmington, MA) weighing 20–30 g were anesthetized by inhaled isoflurane induced at 5% and maintained at 2–3%. The U87Luc cell line was transduced to express luciferase for quantification. The cells were resuspended into 1×10^6 cells/5 μL of media. This cell suspension was then aspirated into a 22 gauge Hamilton syringe and used for injection into the mouse caudate with a stereotactic apparatus with the coordinates from bregma as the origin (A/P: 0 mm, M/L: 2 mm, D/V: 3.5 mm). One week after injection of tumor cells, the mice were imaged using Intravital Imaging Spectroscopy (IVIS) 50 (PerkinElmer). The mice were first anesthetized within an induction chamber using a concentration of 4–5% isoflurane. Next, a subcutaneous injection of 100 μL of luciferin-D Substrate (purchased from Caliper LS and diluted in 35 mL of dH2O with a final concentration of 28.57 mg/mL) was administered. These mice were weighed and then transferred into the imaging chamber where anesthesia was maintained with a concentration of 2–3% isoflurane emitted through nose cones. Five minutes post-injection of luciferin-D, imaging utilizing the IVIS 50 was performed according to manufacturer's protocol. IVIS was run for 1 min and bioluminescence was recorded. Mice were then normalized into groups based upon IVIS counts.

2.12. In vivo injection of cells and nanoparticles

20 mice with an established intracranial tumor were used for this study. Prior to the study, the mice were randomized based on the size of brain tumor in each mouse. The mice were divided into three groups. The first group of 6 mice received an intravenous injection of 1 million T cells suspended in media per animal. The second group of 6 mice received an intravenous injection of clickable BPLP-PLA-NP with DOX suspended in media. The last group of 7 mice received an intravenous injection of 1 million T cells clicked with BPLP-PLA-NP with DOX suspended in media per animal.

2.13. Vector design

The TQM-13-CAR gene [33–35] was synthesized and cloned into the pXL001 vector upon removal of tTR-KRAB using restriction enzymes *Spe*I and *Eco*RI (Genewiz, South Plainfield, NJ, USA). pXL001 was a gift from Sean Palecek (Addgene, Cambridge, MA, USA; plasmid # 26122).

2.14. Lentiviral vector production and CAR T cell production

To generate lentiviruses containing the pXL001-IL13CAR plasmid,

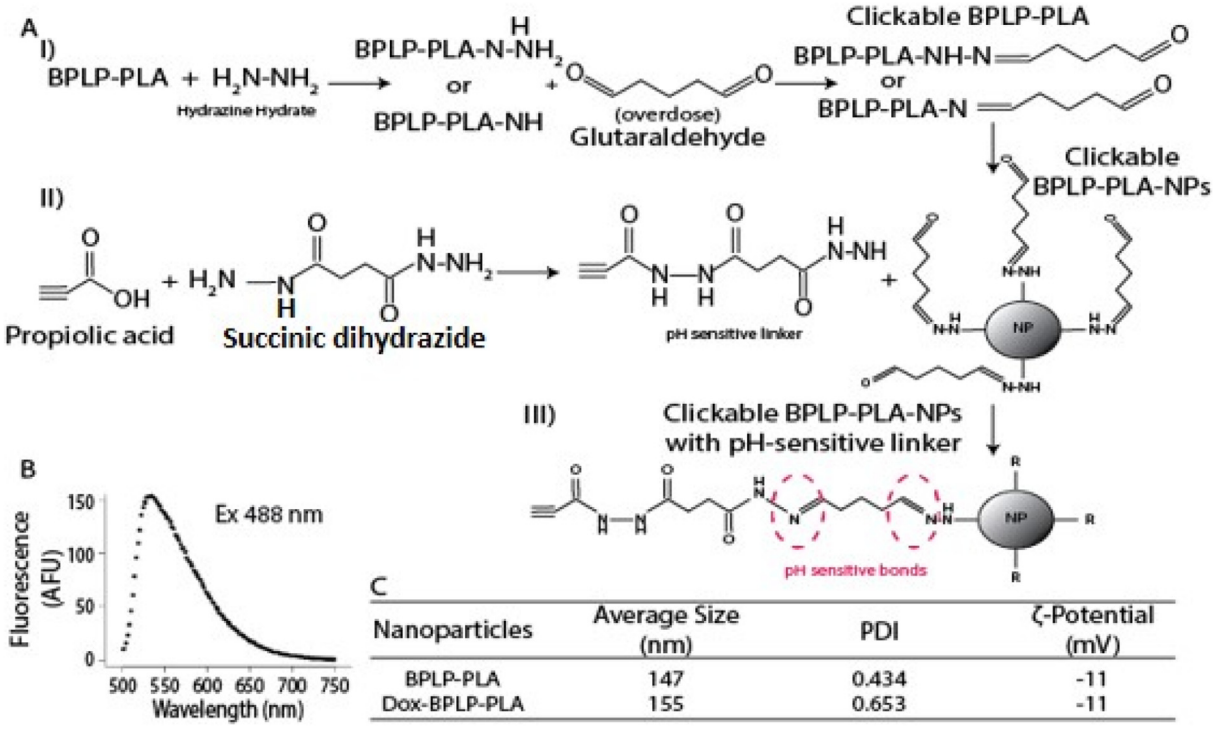

C

Nanoparticles	Average Size (nm)	PDI	ζ-Potential (mV)
BPLP-PLA	147	0.434	-11
Dox-BPLP-PLA	155	0.653	-11

Fig. 1. Fabrication and characterization of BPLP-PLA-NPs. (A) Schematic illustration of (I) clickable BPLP-PLA synthesis, (II) clickable pH-sensitive linkers, and (III) fabrication of BPLP-PLA-NPs with pH-sensitive linkers. **(B)** Emission fluorescence spectra of BPLP-PLA-NP using a 488 nm excitation wavelength. **(C)** Average size, polydispersity index and zeta-potential of BPLP-PLA-NPs and Dox-BPLP-PLA-NPs measured by DLS.

cargo plasmid (pXL001-IL13CAR) and 2nd generation packaging plasmids psPAX2 and pMD2.G were added into OptiMEM from Invitrogen (Invitrogen, Carlsbad, CA, USA; catalog #: 31985070) and incubated at room temperature for 5 min. psPAX2 and pMD2.G were gifts from Didier Trono (Addgene, Cambridge, MA, USA; plasmid # 12260 and 12259). FuGENE HD reagent (Promega, Madison, WI, USA; catalog #: E2311) was added mixed by careful pipetting before incubating at room temperature for 10–15 min. This solution was then added into pre-warmed DMEM +10% FBS to make the transfection media. Medium was changed on 90% confluent HEK293 cells using half of the normal culture volume of transfection medium. Cells were incubated overnight at 37 ˚C and medium was changed the following morning with pre-warmed DMEM +10% FBS using 1.5 times of the normal culture volume. 24, 48, and 72 h after this medium change, virus-containing medium was collected from the cells and the media was changed with pre-warmed DMEM +10% FBS using 1.5 times of the normal culture medium volume. The cells were disposed of after the third collection.

For an unconcentrated virus solution, immediately following collection, the virus containing media was centrifuged for 5 min and the supernatant was collected and stored at −80 ˚C. For concentrated virus solution, the collected virus containing media was stored at 4 ˚C until collection was complete. Virus-containing medium was centrifuged for 5 min and the supernatant was collected. Concentrations were measured using Lenti-X Concentrator (Takara Bio, Mountain View, CA, USA; catalog #: 631231). Activated human T-cells were transduced with these lentiviral vectors.

2.15. T cell immunostaining

For staining and analysis of fixed cells. Cells were pelleted and washed 3 times with DPBS with 0.1% Triton X-100 and 0.5% BSA. Cells were stained with primary and secondary antibodies in DPBS with 0.1% Triton X-100 and 0.5% BSA for 2 h at room temperature. Anti-IL13 primary antibody was used at 1:100 dilution (Santa Cruz Biotech, Dallas, TX, USA; catalog #: sc-1292), donkey anti-goat secondary antibody was used at a 1:1000 dilution (Thermo Fisher Scientific, Waltham, MA, USA; catalog #: A-21432). Cells were pelleted and washed 3 times with DPBS with 0.1% Triton X-100 and 0.5% BSA. Cells spread onto slides, dried, and mounted with Fluorshield + DAPI (Sigma-Aldrich, St. Louis, MO, USA; catalog #: F6057). A Nikon Ti Eclipse epifluorescence microscope was used for image capture and analysis. Coronal brain sections were made at a thickness of 10 μm and fixed in ice-cold 4% paraformaldehyde for 30 min. Slides were washed in 1X DPBS 2 times for 5 min each prior to incubation with primary antibody (Hamster monoclonal anti -CD3 ([1:200], Abcam), rabbit polyclonal anti-Ki67 ([1:200], Abcam) overnight at 4 ˚C. The slides were washed 3 times 5 min each in 1X DPBS. Slides were then incubated with fluorescently-tagged secondary antibody (goat anti-hamster 405 ([1:200], Abcam), and goat anti-rabbit 555 ([1:200], Santa Cruz)) for 1 h at room temperature in the dark. Slides were washed 3 times for 10 min each prior to coverslipping with Fluoro-Gel mounting media. Slides were allowed to dry overnight at room temperature before long-term storage at 4 ˚C. Slides were viewed using an Echo Revolve hybrid microscope with image capture at 20× magnification.

2.16. Western blotting

Cells were washed with DPBS and lysed with Mammalian Protein Extraction Reagent (Thermo Fisher Scientific, Waltham, MA, USA; catalog #: 78501) with 1X Halt's Protease and Phosphatase (Thermo Fisher Scientific, Waltham, MA, USA; catalog #: 78440) by incubation for 3 min. Cell lysate was collected and stored at −80 ˚C until used. Samples were mixed with Laemmli sample buffer (BioRad, Hercules, CA, USA; catalog #: 1610737) at a working concentration of 1X and incubated at 97 ˚C for 5 min. Samples were loaded into a pre-cast MP TGX stain free gel (BioRad, Hercules, CA, USA; catalog #: 4568095) and run at 200V for 30 min in 1X Tris/Glycine/SDS buffer (BioRad). Protein was transferred to a PVDF membrane using a *Trans*-blot Turbo Transfer System (BioRad). The membrane was blocked for 30 min at room temperature in 1X TBST+5% Dry Milk. The membrane was

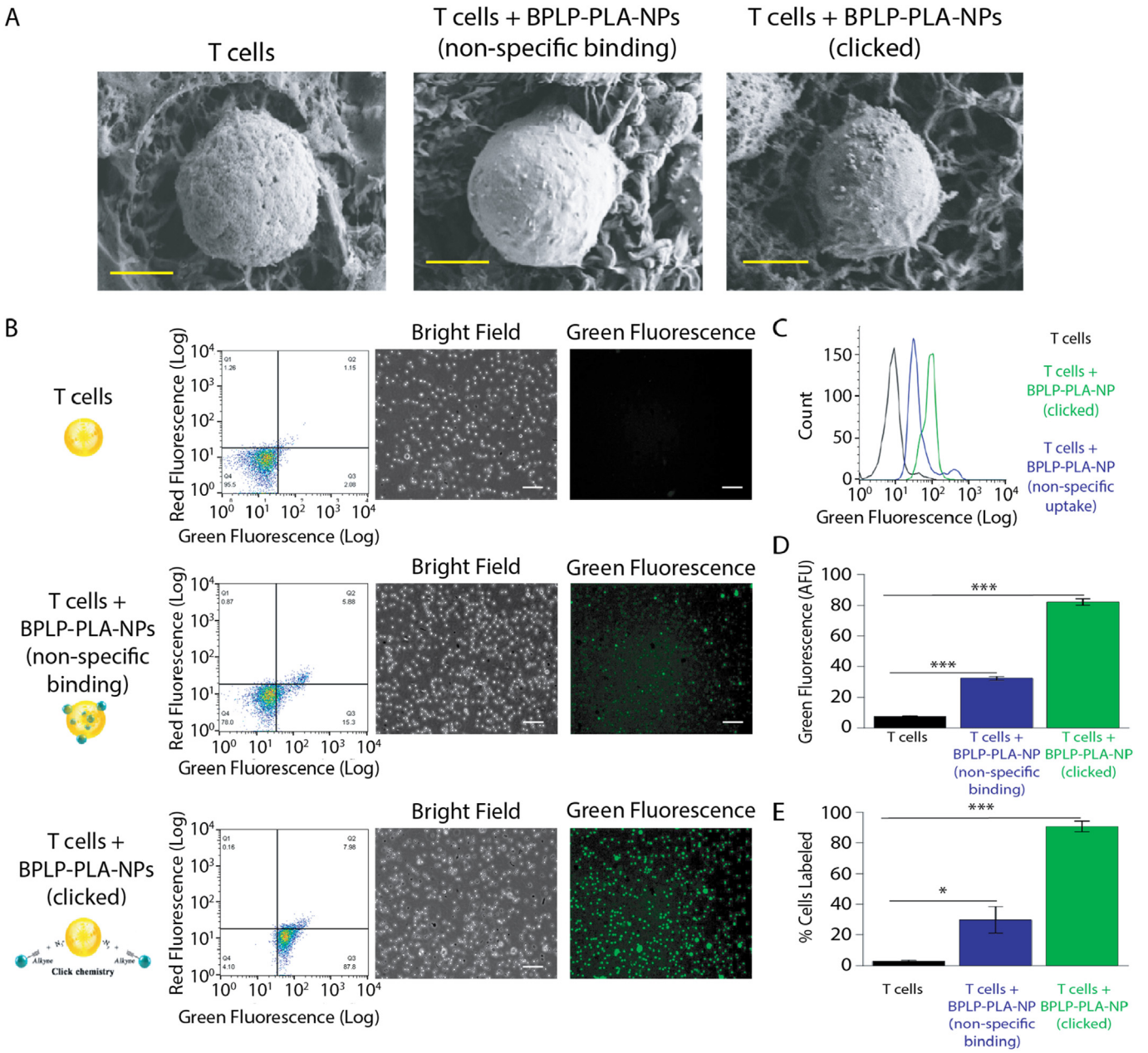

Fig. 2. Clicking of BPLP-PLA-NPs onto T cells. (A) SEM micrographs of T cells, T cells + BPLP-PLA-NPs (non-specific binding) and T cells + BPLP-PLA-NPs (clicked). Scale bar represents 1 μm. **(B)** Flow cytometry data and fluorescent micrographs of T cells, T cells + BPLP-PLA-NPs (non-specific binding) and T cells + BPLP-PLA-NPs (clicked), scale bar represents 50 μm. **(C)** Green fluorescence histograms of the three groups in panel B. **(D)** Green fluorescence intensity quantification of the three groups in panel B. Results represent the mean ± SEM (***$p < 0.001$ in comparison to T cells alone, $n = 3$ for all groups). **(E)** Percentage of cells labeled with NPs of the three groups in panel B. (***$p < 0.001$, *$p < 0.05$ in comparison to T cells alone, $n = 3$ for all groups).

incubated overnight at 4 °C with primary antibodies and for 1 h at room temperature with secondary antibodies in 1X TBST + 5% Dry Milk. The membrane was washed between each antibody exposure with 1X TBST. Chemiluminescence was activated using Clarity Western ECL Substrate (BioRad) and the blot was imaged using a ChemiDoc Touch Imaging System and Image Lab software (BioRad).

2.17. Statistical analysis

- One-way ANOVA with Tukey post hoc tests were used to determine significant differences among indicated groups.

3. Results and discussion

3.1. Characterization of BPLP-PLA-NPs

A biodegradable and biocompatible photoluminescent copolymer (BPLP) was used to fabricate BPLP-PLA-NPs via the single emulsion method as described before (Fig. 1A) [32,34]. As a proof of concept, we have selected doxorubicin as the therapeutic agent for encapsulation inside the NPs. Doxorubicin is known as a potent chemotherapeutic that shows activity against many different types of cancers including glioma [35,36] and has been used widely in nanoparticle-, liposome-, and micelle-based cancer drug delivery systems [37,38]. After nanoparticle fabrication, the fluorescent spectra of BPLP-PLA-NPs in solution was measured to indicate the fluorescent properties of the copolymer. At an

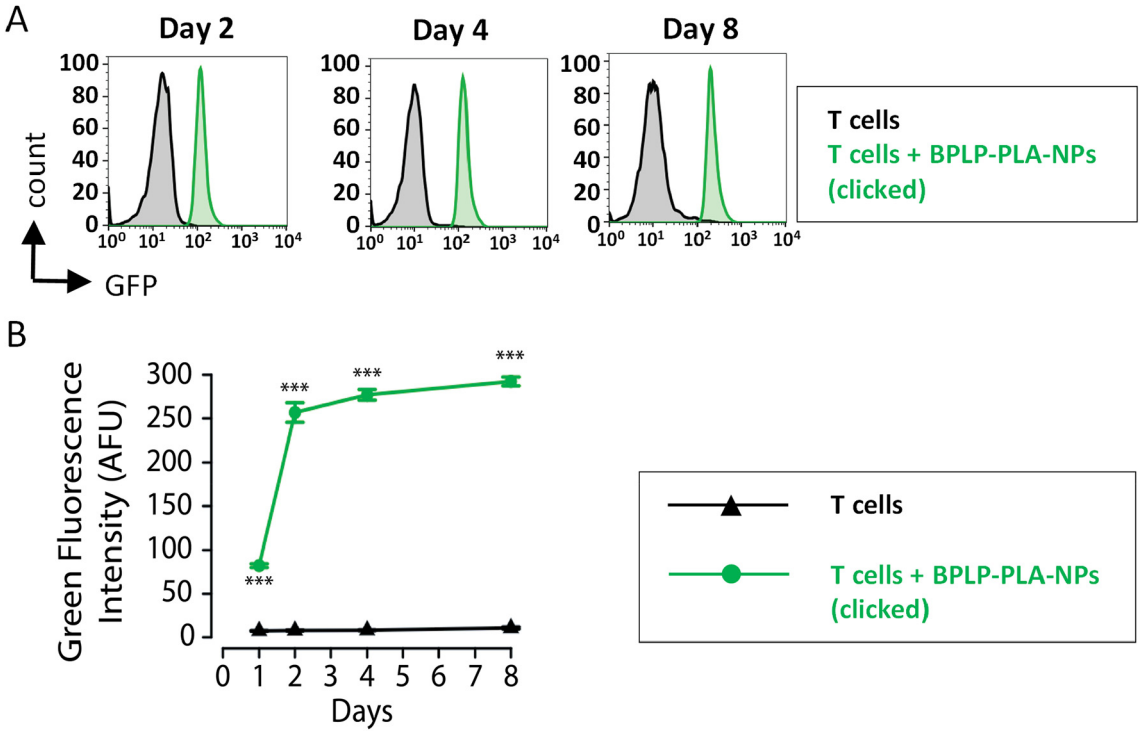

Fig. 3. Stability and fluorescence characterization of BPLP-PLA-NPs clicked T Cells. (A) Flow cytometry analysis of a time-course monitoring on the fluorescence of T cells and T cells + BPLP-PLA-NPs (clicked). **(B)** Green fluorescence intensity quantification of T cells and T cells + BPLP-PLA-NPs (clicked). Results represent the mean ± SEM (***$p < 0.001$ in comparison to T cells alone at equal times, $n = 3$ for all groups).

excitation wavelength of 488 nm, the peak maxima is around 540 nm (Fig. 1B). The quality of empty and drug-loaded NPs was assessed via dynamic light scattering (DLS); the mean diameter was 147 nm for BPLP-PLA-NPs and 155 nm for Dox-BPLP-PLA-NPs; the polydispersity index (PDI) was 0.434 and 0.653, respectively and the zeta-potential for both samples was −11 mV (Fig. 1C).

3.2. Clicking and stability of BPLP-PLA-NPs on T cells

SEM and confocal images of T cells clicked with photoluminescent BPLP-PLA-NPs reveals that the NPs are primarily located on the surface of the cells (Fig. 2A and Fig. S1). To determine the efficiency of the click chemistry method to modify T cells with BPLP-PLA-NPs, three samples were analyzed using flow cytometry (Fig. 2B). T cells clicked with BPLP-PLA-NPs exhibited significantly higher fluorescence intensity in the green channel compared to the T cells alone and the T cells incubated with BPLP-PLA-NPs but not functionalized with azide sugar. The latter group is referred to as the non-specific binding group. The difference between the three samples is represented in their Q2 and Q3 areas. T cells clicked with NPs showed 2.5 times higher signal in the green channel compared with the T cells that bind NPs in a non-specific manner (Fig. 2C–D). The reaction efficiency was very high, 96% of T cells were labeled with BPLP-PLA-NPs in the clicked group compared to only 25% for the non-specific binding group (Fig. 2E). The incubation time with NPs allotted for both groups (non-specific binding and clicked) was kept consistent at 30 min for a direct comparison. This higher NP loading capacity using click chemistry is expected to increase the drug delivery efficiency as well.

The attachment of BPLP-PLA-NPs via an acid-cleavable hydrazine linkage has been proved to be effective in enhancing the delivery of doxorubicin because the hydrazine bonds can be cleaved under the mild acidic conditions of the tumor microenvironment to release free BPLP-PLA-NPs [41,42]. The pH-sensitive cleavage of clickable BPLP-PLA-NPs from T cells has been tested in acidic and neutral solutions (Fig. S2). SEM images of the cells in both cases showed that lowering pH cleaved the NPs from the cells very effectively in acidic conditions. Thus, the current system will benefit from tumor microenvironments in releasing the drug-loaded NPs in the tumor site. Additionally, the surface conjugation of NPs on T cells can minimize the side effects to the cells in contrast to loading particles inside the cells.

BPLP-PLA-NPs clicked onto T cells are retained for at least 8 days showing that the hydrazine linkage is stable under physiological conditions (Fig. 3A). A time-course experiment was conducted to analyze the fluorescence intensity of T cells alone and T cells clicked with BPLP-PLA-NPs using flow cytometry. As expected, the fluorescence of T cells alone did not change over time. In contrast, T cells clicked with BPLP-PLA-NPs show progressively higher fluorescence. Quantification of green fluorescence intensity revealed a significant difference between the two groups (Fig. 3B). Surprisingly, even though samples were repeatedly washed right after the clicking reaction and any unbound NPs were washed away, the fluorescence intensity for the BPLP-PLA-NPs clicked group stayed high over time. This effect was replicated when BPLP-PLA-NPs alone were resuspended in media and incubated for 8 days. Green fluorescence intensity was measured on days 1, 2, 4 and 8.

3.3. Key physiological functions of T cells are not altered following BPLP-PLA-NP clicking

The proposed approach for drug delivery relies on the ability of T cells to conduct their normal physiological functions following BPLP-PLA-NP clicking. Cells have to be able to interact with the endothelium and migrate across the BBB to deliver their cargo to solid tumors located in the brain. Initially, T cell proliferation after BPLP-PLA-NPs clicking was assessed via incorporation of a neutral red dye that is taken up by viable cells and stored in the lysosomes until cells are lysed. Following solubilization of the dye, absorbance was measured for T cells alone and T cells clicked with BPLP-PLA-NPs at days 1, 2, 4 and 8. The results showed no significant difference between cell proliferation of T cells alone compared to T cells clicked with BPLP-PLA-NPs over a period of 8 days (Fig. 4A), confirming that the BPLP-PLA polymer is

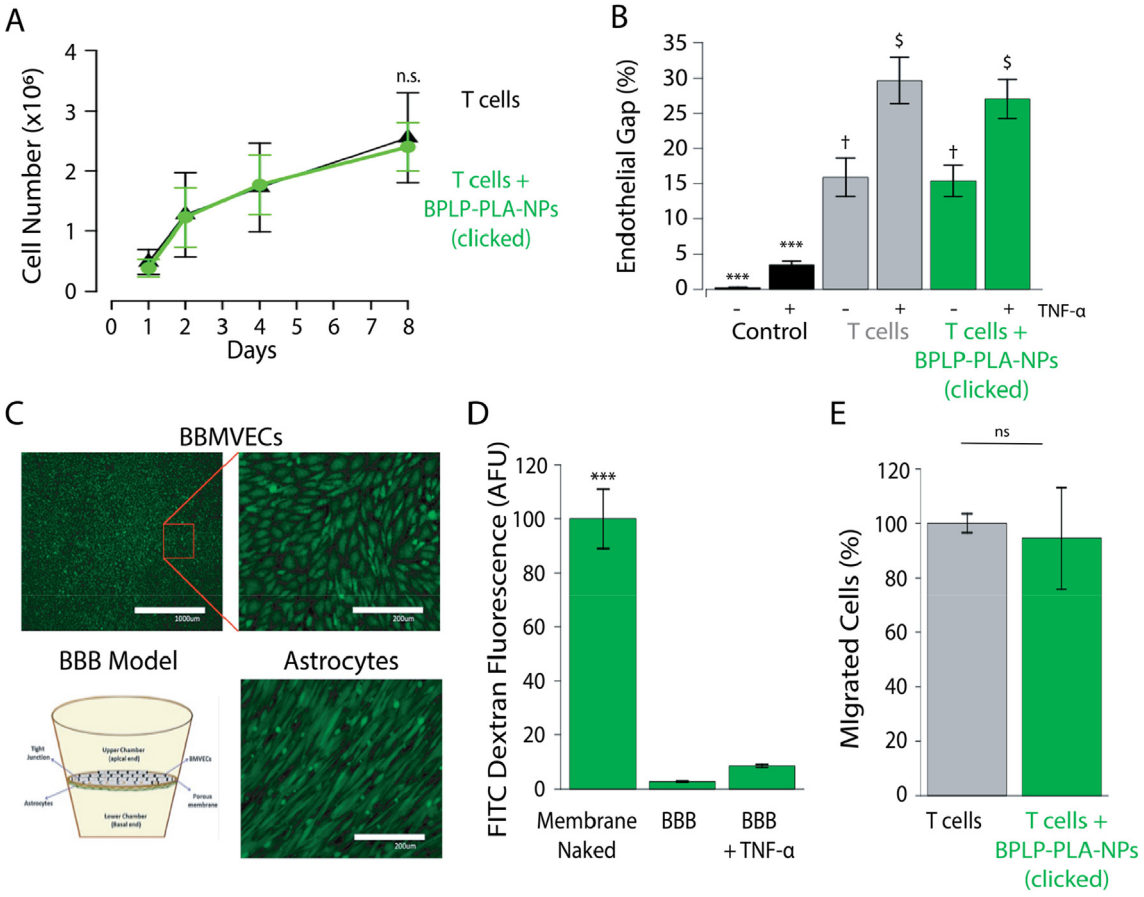

Fig. 4. Normal physiological functions of immune cells are not altered following clicking of BPLP-PLA-NPs. (A) Proliferation of T cells and T cells + BPLP-PLA-NPs (clicked) over 8 days. Results represent the mean ± SEM (ns - no significant difference, n = 4 for both groups). **(B)** Gap formation by T cells and T cells + BPLP-PLA-NPs (clicked) on monolayers of BBMVECs. Results represent the mean ± SEM (***, †, $ $p < 0.001$ in comparison to control group, no significant difference between groups with same symbols, n = 3 for all groups). **(C)** Fluorescent micrographs, cartoon of the BBB model *in vitro*. Scale bar represents 1000 μm on the left image and 200 μm on the right images. **(D)** Quantification of diffusion of FITC-Dextran MW 40 kDa across the BBB model. Results represent the mean ± SEM (***$p < 0.001$ in comparison to membrane naked, n = 3 for all groups). **(E)** Quantification of T cells and T cells + BPLP-PLA-NPs (clicked) that migrated *in vitro* in response to CXCL-12 (bottom). Results represent the mean ± SEM (ns - not statistically significant difference, n = 3 for both groups).

biocompatible.

T cells have a natural ability to cross the BBB under certain physiological and pathological conditions [43]. Prior to their transmigration through the BBB, they first need to form intercellular gaps in the endothelium [44]. To evaluate the potential of using T cells for the delivery of drug-encapsulating NPs through the BBB, we developed an *in vitro* assay where we tested the ability of T cells to disrupt the endothelial barrier. The stimulation of endothelial cells with TNF-α or other pro-inflammatory cytokines promotes the expression of specific cell adhesion molecules on endothelial cells. Previous studies in endothelial cells have shown that the treatment with TNF-α increases the expression of VCAM-1 [45] and ICAM-1 [46] receptors, as well as E-selectin [47]. These molecules are key players that mediate interactions between endothelial cells and immune cells. The results have shown that immune cells retain the ability to disrupt the endothelium, following the click reaction (Fig. 4B). A significant disruption of the endothelial barrier was observed in monolayers co-cultured with T cells and T cells clicked with BPLP-PLA-NPs (~30%) compared to the control group without immune cells (~4%). There was no statistically significant difference in gap formation between T cells and T cells clicked with BPLP-PLA-NPs. This result indicates that the clicked BPLP-PLA-NPs do not interfere with cell-cell interactions between immune cells and the endothelium. Furthermore, T cells exhibited the ability to form gaps on monolayers of brain endothelial cells while maintaining normal cell proliferation and viability, which indicates that the click chemistry approach is compatible with physiological cell functions.

In order to assess the migration function of T cells through the BBMVECs, we successfully established an *in vitro* BBB model using BBMVECs and astrocytes on a porous membrane (Fig. 4C). The barrier function of the BBB model was confirmed by measuring the diffusion of FITC-Dextran MW 40 kDa across the barrier (Fig. 4D). Compared to the naked filter, diffusion of FITC-Dextran across the BBB was only 3%; when the endothelium was activated with TNF-α, diffusion increased to 8.5%. This shows that the BBB model *in vitro* restricted the passage of small molecules and responded to cytokine stimuli, resembling the conditions *in vivo*. Using this system, we tested the extravasation ability of T cells following the clicking reaction. Our *in vitro* studies showed that the T cells carrying clickable BPLP-PLA-NPs transmigrated across the BBB and efficiently delivered NPs to the basal chamber under pseudo-inflammatory conditions created using CXCL-12 as a chemoattractant. CXCL-12 was used in this study as it has been shown to be highly expressed by primary brain tumors [48] and modulate the immune response [45–47]. T cells alone or clicked with BPLP-PLA-NPs were incubated on top of the BBB model and extravasation was assessed to confirm that conjugation with BPLP-PLA-NPs does not impede cell motility. After 4 h, T cells were collected from the bottom chamber, counted and compared across the samples (Fig. 4E). The results were normalized with respect to the T cell group. As shown, the percentage of migrated cells did not change significantly after they were clicked with BPLP-PLA-NPs. This indicates that BPLP-PLA-NPs do not alter the

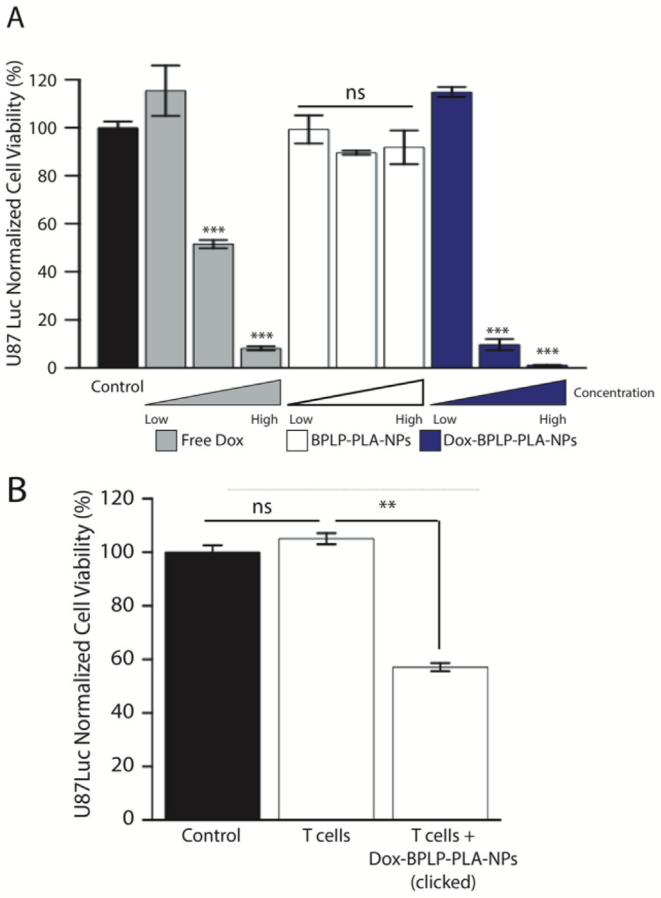

Fig. 5. Cytotoxic effect of Dox-BPLP-PLA-NPs clicked onto T cells. (A) Viability of U87Luc cells after 48 h treatment with free doxorubicin, BPLP-PLA-NPs alone or Dox-BPLP-PLA-NPs alone. Results represent the mean ± SEM. Statistical analysis shows significant difference with respect to control group (***$p < 0.001$, n.s – no significant difference between groups, $n = 3$ for all groups). **(B)** Viability of U87Luc cells after 48 h treatment with media alone (control), T cells alone or T cells + Dox-BPLP-PLA-NPs (clicked). Results represent the mean ± SEM. Statistical analysis shows significant difference with respect to T cells alone (**$p < 0.01$, n.s - no significant difference between groups, $n = 3$ for all groups).

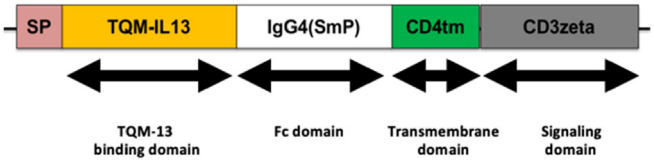

Fig. 6. Schematic for TQM-IL13 CAR. It includes a signal peptide (SP), TQM-13 as an extracellular domain (TQM-IL13), an Fc domain [IgG4 (SmP)], a transmembrane domain (CD4tm), and an intracellular signal transduction domain CD3-ζ.

ability of T cells to extravasate through the BBB and target cancer cells. As an additional negative control, BPLP-PLA-NPs alone were incubated in the top chamber. After 4 h, no NPs were detected in the bottom chamber when the BBB was grown on the membrane (Fig. S3). These results suggest that our approach can offer significant advantages over traditional nanoparticle drug delivery systems in overcoming the BBB.

3.4. Cytotoxic effects of CTNDDS

Doxorubicin was used as the chemotherapeutic agent for encapsulation inside BPLP-PLA-NPs. To use the single emulsion method for BPLP-PLA-NPs fabrication without major modifications, doxorubicin was first diluted in DMSO and incorporated into the organic phase during the process. The encapsulation efficiency was 28%. To investigate the cytotoxic effects of CTNDDS on glioblastoma cells, we used U87 cells labeled with luciferase, termed U87Luc.

Initially, U87Luc cells were treated with increasing concentrations of free doxorubicin (10, 100 and 1000 ng/ml), BPLP-PLA-NPs alone or Dox-BPLP-PLA-NPs (0.4, 4 and 40 μg/ml) for 48 h. The concentrations of BPLP-PLA-NPs and Dox-BPLP-PLA-NPs were calculated as equivalent doses to free doxorubicin based on the encapsulation efficiency of the drug on NPs (1.4 mg Dox/mg NP). After the incubation period, the viability of U87Luc cells was inferred from the luciferase activity in viable cells remaining. As expected, the results show that only free doxorubicin and Dox-BPLP-PLA-NPs are toxic to the cells (Fig. 5A). In contrast, BPLP-PLA-NPs alone do not decrease cell viability over the same period of time. This again confirms that the BPLP polymer is biocompatible and does not have any observable cytotoxic effects. Further, these results indicate that chemotherapeutic agents can be encapsulated inside BPLP-PLA-NPs and subsequently released in the presence of tumor cells. Interestingly, BPLP-PLA-NPs at medium and high concentrations showed higher toxicity compared to free doxorubicin. This result might reflect a higher BPLP-PLA-NP uptake by U87Luc cells versus doxorubicin free flowing in the media.

To show that Dox-BPLP-PLA-NPs retain their cytotoxic capability after the clicking reaction, T cells were either unmodified or clicked with Dox-BPLP-PLA-NPs and co-cultured with U87Luc cells for 48 h. The ratio of T cells to U87Luc cells was held constant at 1 to 1. After 48 h, about 50% cytotoxicity was observed in the group clicked with Dox-BPLP-PLA-NPs compared to the unmodified control (Fig. 5B).

3.5. Delivery of CTNDDS to glioblastoma in vivo

To efficiently deliver BPLP-PLA-NPs into glioblastoma tumors, instead of untransduced primary T cells, a genetically-modified TQM-13-CAR T cell version was used. The CAR molecule consisted of a signal peptide (SP), TQM-13 as an extracellular domain (TQM-IL13), an Fc domain [IgG4 (SmP)], a transmembrane domain (CD4tm) and an intracellular signal transduction domain CD3-ζ (Fig. 6). T cells were transduced with a concentrated lentivirus and incubated with antibiotics to select for positive transduced cells. During this expansion, the TQM-13-CAR-T cell population increased from 3% after transduction to 65%. To demonstrate that the TQM-13-CAR T cells could access the tumors *in vivo*, following transduction, TQM-13-CAR T cells were administered to nude mice via tail vein injection (Fig. 7C). The mice were sacrificed 24 h after injection. The brains were harvested and processed for immunohistochemistry. Brain sections were stained with anti-Ki67 and anti-CD3 for tumor and T cell detection, respectively (Fig. 7D–F). TQM-13-CAR modified T cells were observed within the tumor. As a comparison, untransduced T cells were also injected but they were not detected in the tumors (Fig. 7G–H).

Next, to test the feasibility of using our CTNDDS system *in vivo*, TQM-13-CAR T cells clicked with BPLP-PLA-NPs ($n = 3$) and BPLP-PLA-NPs alone ($n = 3$) were injected into three groups of nude mice bearing intracranial brain tumors. Our results confirmed that BPLP-PLA-NPs can be stably attached to the surface of CAR T cells. Approximately 24 h after the intravenous injection, the brains were harvested, fixed, and stained with anti-CD3 and anti-Ki67 antibodies. In the group of mice that received TQM-13-CAR T cells clicked with BPLP-PLA-NPs, BPLP-PLA-NPs (green fluorescence signal) were co-localized with the brain tumor cells stained with the proliferating marker, Ki67, in red (Fig. 8A–E). CD3 marker was also detected throughout the tumor. In the group of mice that received BPLP-PLA-NPs alone, no BPLP-PLA-NPs were detected in the brain tumor (Fig. 8F). TQM-13 CAR T cells clicked with BPLP-PLA NPs delivered significantly more BPLP-PLA-NPs into the brain tumors compared to injections of BPLP-PLA-NPs alone. These results suggest that TQM-13-CAR T cells loaded with NPs have

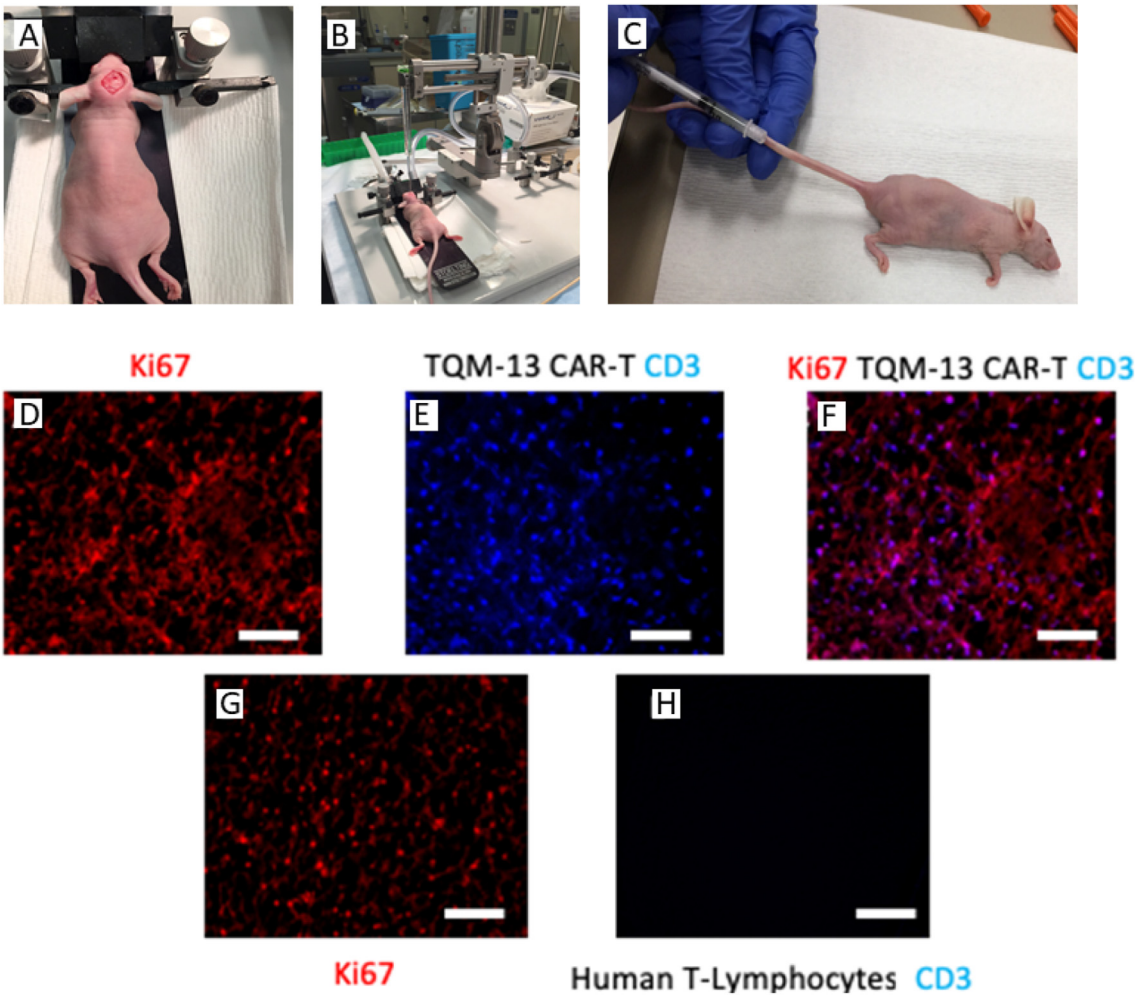

Fig. 7. TQM-13 CAR-T cells infiltrate mouse intracranial tumors. (A) Shows the stereotaxic setup in which the mouse is placed for the surgical procedure of preparing intracranial model. **(B)** Shows the setup in which U87Luc cells are intracranially injected. **(C)** Shows a nude mouse tail-injected with TQM-13 CAR-T cells. **(D–H)** These are a series of representative images from the mouse intracranial tumor model using u87 cells to establish the tumor. **(D)** Demonstrates establishment of a proliferative tumor within the brain with staining for Ki67. **(E)** Demonstrates the presence of human T cells (detected with CD3) in the tumor 24 h after injection. **(F)** Overlay from A and B demonstrates that TQM-13 CAR-T human T cells are found within the tumor. **(G–H)** Show slices from a tumor bearing mouse that received untransduced T cells. **(G)** Demonstrates establishment of a proliferative tumor within the brain with staining with Ki67. **(H)** Shows that untransduced human T cells are not detected in the tumor 24 h after injection. Scale bars represent 70 μm.

the potential to deliver therapeutic drugs into solid tumors. This approach is a new strategy to overcome the immunosuppressive tumor microenvironment because it does not depend on the cytotoxic ability of T cells, but rather relies on the infiltration ability of T cells for delivery of the therapeutic drug. Immunotherapies for GBM often face several well-known limiting factors, including tumor heterogeneity, low tumor mutational burden (TMB), low levels of T cell infiltration, and potent immunosuppressive capabilities [51,52]. To overcome these challenges and enhance the effect of existing cancer immunotherapies, the inherent fluorescent BPLP-PLA-NPs may be used as backpacks to carry not only antitumor drugs, but also immunostimulatory molecules such as cancer antigens and adjuvants, and additional MRI imaging agents that enable tracing of the targeting and delivery process *in vivo*. Additionally, the antigenic heterogeneity exhibited by GBM could be combated by targeting multiple antigens either simultaneously or in sequence with CAR molecules. Therefore, it might be beneficial to study the effect of multi-targeted CARs either simultaneously or sequentially for success in clinical applications.

4. Conclusions

Our system offers the following advantages in comparison with a traditional chemotherapy for brain cancer: 1) reduces systemic toxicity and achieves higher drug bioavailability at the target site by encapsulating the antitumor drug inside biodegradable polymeric NPs, 2) offers a facile, efficient single step clicking of NPs to the surface of T cells, 3) enhances targeted delivery of therapeutic NPs by using human T cells as living drug carriers or backpacks, 4) specifically targets and kills the brain cancer cells by utilizing high-affinity TQM-13 CAR T cells, and 5) cleaves and releases the NPs from the cells via its pH-sensitive linkers in the acidic tumor microenvironment. Although the therapeutic effects of our CTNDDS system for cancer treatment is not the focus of this work and will be our immediate future research endeavor, this cell and nanoparticle delivery platform technology is expected to become an important tool to impact multiple disciplines, including immunology, drug delivery, biomaterials, and cancer biology and lead to the development of cell-based therapies for cancer management and regenerative medicine.

Declaration of competing interest

Dr. Yang and The Pennsylvania State University have a financial interest in Acuitive Technologies, Inc. and Aleo BME, Inc. These

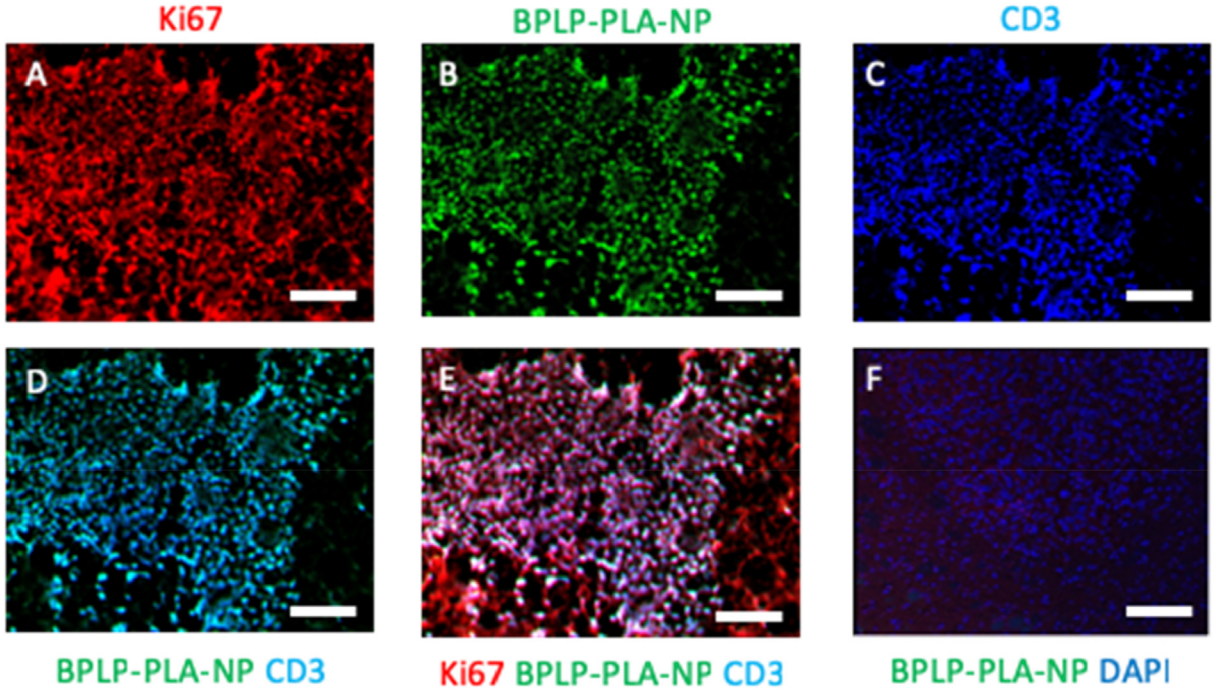

Fig. 8. TQM-13 CAR-T modified cells clicked with BPLP-PLA NPs infiltrate tumor tissue in the murine intracranial model. (A) Demonstrates establishment of a proliferative tumor within the brain with KI67 staining. **(B)** Indicates the presence of fluorescently labeled BPLP-PLA NP in the tumor after intravenous injection of TQM-13 CAR-T clicked with BPLP-PLA NP cells. This figure takes advantage of the inherent fluorescence of the NPs (green). **(C)** Demonstrates the presence of TQM-13 CAR-T human T cells in the tumor. **(D)** Overlay from B and C demonstrates that TQM-13 CAR-T cells clicked with BPLP are associated with the human T cells. **(E)** Affirms that BPLP-PLA NP clicked to TQM-13 CAR-T cells were delivered to the intracranial tumor (overlay includes the presence of Ki67 staining). **(F)** Demonstrates that there are no detectable NPs in the tumor when the NPs are injected without clicking to the T cells. Scale bars represent 70 μm.

interests have been reviewed by the University's Institutional and Individual Conflict of Interest Committees and are currently being managed by the University.

Acknowledgments

This work was supported in part by PA Tobacco Settlement Fund (Grant 4100062216, to C.D., J.Y. J.C). We are grateful for the funding support from the National Institutes of Health Award (AR072731, to J.Y. and EB026035, to X.L.) and the National Science Foundation (NSF) Award (CBET-BME1330663, to C.D.). The authors sincerely acknowledge Dr. Justin Pritchard from the Biomedical Engineering Department at Penn State for insightful discussions and helpful advice regarding CAR T cell technologies. The authors also would like to acknowledge the instrument help from the Penn State Microscopy and Cytometry Facility at University Park, PA and Dr. Joseph Choi of Einstein Hospital for insightful comments.

Appendix A. Supplementary data

Supplementary data related to this article can be found at https://doi.org/10.1016/j.bioactmat.2020.04.011.

References

[1] R.K. Jain, E. Di Tomaso, D.G. Duda, J.S. Loeffler, A.G. Sorensen, T.T. Batchelor, Angiogenesis in brain tumours, Nat. Rev. Neurosci. 8 (8) (2007) 610–622.
[2] P.D. Delgado-Lopez, E.M. Corrales-Garcia, Survival in glioblastoma: a review on the impact of treatment modalities, Clin. Transl. Oncol. 18 (11) (2016) 1062–1071.
[3] M.M. Mrugala, Advances and challenges in the treatment of glioblastoma: a clinician's perspective, Discov. Med. (2013).
[4] D. Orringer, et al., Extent of resection in patients with glioblastoma: limiting factors, perception of resectability, and effect on survival, J. Neurosurg. 117 (5) (2012) 851–859.
[5] E. Klein, S. Becker, E. Svedmyr, M. Jondal, F. Vanky, Tumor infiltrating lymphocytes, Ann. N. Y. Acad. Sci. 276 (1) (1976) 207–216.
[6] S.A. Rosenberg, et al., Use of tumor-infiltrating lymphocytes and IL-2 in the immunotherapy of patients with metastatic melanoma, N. Engl. J. Med. 319 (25) (1988) 1676–1680.
[7] A.D. Fesnak, B.L. Levine, C.H. June, Engineered T cells: the promise and challenges of cancer immunotherapy, Nat. Rev. Canc. 16 (9) (2016) 566–581.
[8] M. Sadelain, R.J. Brentjens, I. Rivière, The basic principles of chimeric antigen receptor design, Canc. Discov. 3 (4) (2013) 388–398.
[9] J.N. Kochenderfer, et al., Eradication of B-lineage cells and regression of lymphoma in a patient treated with autologous T cells genetically engineered to recognize CD19, Blood 116 (20) (2010) 4099–4102.
[10] D. Akhavan, D. Alizadeh, D. Wang, M.R. Weist, J.K. Shepphird, C.E. Brown, CAR T cells for brain tumors: lessons learned and road ahead, Immunol. Rev. (2019).
[11] P. Sharma, J.P. Allison, The future of immune checkpoint therapy, Science 348 (6230) (2015) 56–51.
[18] C.E. Brown, et al., Regression of glioblastoma after chimeric antigen receptor T-cell therapy, N. Engl. J. Med. 375 (26) (2016) 2561–2569.
[19] C.E. Brown, et al., Bioactivity and safety of IL13Rα2-redirected chimeric antigen receptor CD8+ T cells in patients with recurrent glioblastoma, Clin. Canc. Res. 21 (18) (2015) 4062–4072.
[20] D.M. O'Rourke, et al., A single dose of peripherally infused EGFRvIII-directed CAR T cells mediates antigen loss and induces adaptive resistance in patients with recurrent glioblastoma, Sci. Transl. Med. 9 (399) (2017) eaaa0984.
[21] V. Nguyen, C. Hollingsworth, W. Debinski, A. Mintz, A novel ligand delivery system that targets the IL13Rα2 tumor-restricted biomarker, Neuro Oncol. 14 (10) (2012) 1239–1253.
[22] A.B. Madhankumar, et al., Efficacy of interleukin-13 receptor-targeted liposomal doxorubicin in the intracranial brain tumor model, Mol. Canc. Therapeut. 8 (3) (2009) 648–654.
[23] W. Debinski, D.M. Gibo, Molecular expression analysis of restrictive receptor for interleukin 13, a brain tumor-associated cancer/testis antigen, Mol. Med. 6 (5) (2000) 440–449.
[24] D.A. Wainwright, P. Nigam, B. Thaci, M. Dey, M.S. Lesniak, Recent developments on immunotherapy for brain cancer, Expet Opin. Emerg. Drugs 17 (2) (2012).
[25] J. Hu, et al., Fluorescence imaging enabled poly(lactide-co-glycolide), Acta Biomater. 29 (2016) 307–319.
[26] D. Shan, J.T. Hsieh, X. Bai, J. Yang, Citrate-based fluorescent biomaterials, Adv. Healthc. Mater. 7 (2018).
[27] D. Shan, et al., Polymeric biomaterials for biophotonic applications, Bioactive Mater. (2018) 434–445.
[28] C. Ma, E. Gerhard, D. Lu, J. Yang, Citrate chemistry and biology for biomaterials design, Biomaterials 178 (2018) 383–400.
[29] C. Ma, E. Gerhard, Q. Lin, S. Xia, A.D. Armstrong, J. Yang, In vitro cytocompatibility evaluation of poly(octamethylene citrate) monomers toward their use in orthopedic regenerative engineering, Bioact. Mater. 3 (2018) 19–27.

[30] L. Young, J. Sung, J.R. Masters, Detection of mycoplasma in cell cultures, Nat. Protoc. 5 (2010) 929–934.
[31] J. Yang, et al., Development of aliphatic biodegradable photoluminescent polymers, Proc. Natl. Acad. Sci. 106 (28) (2009) 10086–10091.
[32] Z. Xie, et al., Development of intrinsically photoluminescent and photostable polylactones, Adv. Mater. 26 (2014) 4491–4496.
[33] A.B. Madhankumar, A. Mintz, W. Debinski, Interleukin 13 mutants of enhanced avidity toward the glioma-associated receptor, IL13Rα2, Neoplasia 6 (1) (2004) 15–22.
[34] A.B. Madhankumar, A. Mintz, W. Debinski, Alanine-scanning mutagenesis of alpha-helix D segment of interleukin-13 reveals new functionally important residues of the cytokine, J. Biol. Chem. 277 (November 8) (2002) 43194–43205.
[35] V. Nguyen, et al., A novel ligand delivery system to non-invasively visualize and therapeutically exploit the IL13Rα2 tumor-restricted biomarker, Neuro Oncol. 14 (10) (2012) 1239–1253.
[36] Z. Xie, et al., Immune cell-mediated biodegradable theranostic nanoparticles for melanoma targeting and drug delivery, Small 13 (10) (2017) 1–10.
[37] L.L. Muldoon, E.A. Neuwelt, BR96-DOX immunoconjugate targeting of chemotherapy in brain tumor models, J. Neuro Oncol. 65 (1) (2003) 49–62.
[38] E.M. Kemper, W. Boogerd, I. Thuis, J.H. Beijnen, O. van Tellingen, Modulation of the blood-brain barrier in oncology: therapeutic opportunities for the treatment of brain tumours? Canc. Treat Rev. 5 (30) (2004) 415–423.
[41] R. Patil, et al., Cellular delivery of doxorubicin via pH-controlled hydrazone linkage using multifunctional nano vehicle based on poly(??-L-malic acid), Int. J. Mol. Sci. 13 (9) (2012) 11681–11693.
[42] K. Ulbrich, T. Etrych, P. Chytil, M. Jelínková, B. Říhová, Antibody-targeted polymer-doxorubicin conjugates with pH-controlled activation, J. Drug Target. 12 (8) (2004) 477–489.
[43] Y. Chen, L. Liu, Modern methods for delivery of drugs across the blood-brain barrier, Adv. Drug Deliv. Rev. 64 (7) (2012) 640–665.
[44] R. Alon, J.D. van Buul, Leukocyte breaching of endothelial barriers: the actin link, Trends Immunol. 38 (8) (2017) 606–615.
[45] D. Wong, K. Dorovini-Zis, Expression of vascular cell adhesion molecule-1 (VCAM-1) by human brain microvessel endothelial cells in primary culture, Microvasc. Res. 49 (3) (1995) 325–339.
[46] S.K. Lo, J. Everitt, J. Gu, A.B. Malik, Tumor necrosis factor mediates experimental pulmonary edema by ICAM-1 and CD18-dependent mechanisms, J. Clin. Invest. 89 (3) (1992) 981–988.
[47] D. Wong, K. Dorovini-Zis, Regulation by cytokines and lipopolysaccharide of E-selectin expression by human brain microvessel endothelial cells in primary culture, J. Neuropathol. Exp. Neurol. 55 (2) (1996) 225–235.
[48] S. Barbero, et al., Stromal cell-derived factor 1α stimulates human endometrial carcinoma cell growth through the activation of both extracellular signal-regulated kinase 1/2 and Akt, Canc. Res. 63 (2003) 1969–1974.
[51] K. Dunussi-Joannopoulos, et al., Efficacious immunomodulatory activity of the chemokine stromal cell-derived factor 1 (SDF-1): local secretion of SDF-1 at the tumor site serves as T-cell chemoattractant and mediates T-cell-dependent anti-tumor responses, Blood 100 (5) (2002) 1551–1558.
[52] T.R. Hodges, et al., “Mutational burden, immune checkpoint expression, and mismatch repair in glioma: implications for immune checkpoint immunotherapy,” *Neuro*, Oncol. 19 (8) (2017) 1047–1057.